

Article

Photocatalytic Degradation of Atenolol by TiO₂ Irradiated with an Ultraviolet Light Emitting Diode: Performance, Kinetics, and Mechanism Insights

Zhilin Ran ^{1,†}, Liping Wang ^{2,†}, Yuanhang Fang ³, Cong Ma ^{4,*} and Shaofeng Li ^{5,*}

¹ Institute of Innovational Education Research, School of Transportation and Environment, Shenzhen Institute of Information Technology, Shenzhen 518172, China; ranzl@szit.edu.cn

² School of Environmental Science and Engineering, Chang'an University, Xi'an 710064, China; lipingwang1528@chd.edu.cn

³ Shenzhen Water Affairs (Group) Co. Ltd., Shenzhen 518033, China; yaom@szit.edu.cn

⁴ State Key Laboratory of Separation Membranes and Membrane Processes, School of Environmental Science and engineering, Tiangong University, Tianjin 300387, China

⁵ Department of Building and Environmental Engineering, Shenzhen Polytechnic, Shenzhen 518055, China

* Correspondence: hit.macong@gmail.com (C.M.); lisf@szit.edu.cn (S.L.); Tel.: +86-15122382805 (C.M.); +86-13622353215 (S.L.)

† These authors contributed equally to this work, which are co-first authors.

Received: 4 September 2019; Accepted: 21 October 2019; Published: 23 October 2019



Abstract: Batch experiments were performed to investigate the effect of several environmental factors on atenolol (ATL) degradation efficiency, including catalyst crystal phase (anatase TiO₂, rutile TiO₂, and mixed phase), catalyst dosage, UV-LED wavelength and intensity, co-existing anions, cations, and pH. The mixed phase (2 g/L) exhibited the best photocatalytic activity at 365 nm, with ATL (18.77 μM) completely oxidized within 1 h. These results suggest that: (i) The mixed phase exhibits the highest activity due to its large specific surface area and excellent charge separation efficiency. (ii) ATL can be effectively degraded using mixed phase TiO₂ combined with UV-LED technology and the ATL degradation efficiency could reach 100% for 60 min; (iii) ATL photodegradation was more effective under 365 nm UV-LED than 254 nm, which was caused by the effect of light-induced charge separation; (iv) the ATL Degradation efficiency(De) decreased with an increase in initial ATL concentrations; and (v) co-existing anions and cations had different effects on the ATL De, mainly by changing the concentration of hydroxyl radicals. Considering that UV-LED is more energy-saving and environmentally friendly, and commercial TiO₂ is cheap and easy to obtain, our research provides feasibility for practical application.

Keywords: ultraviolet light emitting diode; advanced oxidation process; nano titanium dioxide; photocatalysis; hydroxyl radical; atenolol

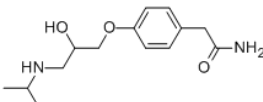
1. Introduction

Due to the development of human sanitation, health, and cosmetic industries in recent decades, pharmaceuticals and personal care products (PPCPs) are now used worldwide, with trace environmental contamination commonly reported due to the production, use, and disposal of livestock medicines, pesticides, human medicines, PPCPs, and their metabolites [1]. PPCPs and their metabolites are now regularly reported in the aquatic environment worldwide and as most PPCP substances are quite stable with complex structures, they cannot be easily absorbed and digested by biological organisms, resulting in environmental persistence and an increased potential hazard to both human and environmental health [2,3]. The enrichment of these chemical contaminants in aquatic environments

may also contribute to antibiotic resistance and the spread of resistance genes, which potentially poses a serious threat to the whole ecosystem [4–6]. Therefore, it is imperative to remove PPCPs from the aquatic environment, to reduce the risk they pose to all biota.

Atenolol (ATL) is a representative PPCPs compound which has been used for nearly 40 years and is associated with cardiovascular disease as a selective β_1 adrenergic receptor blocker [7]. ATL has also been proven to inhibit the growth of human embryonic cells and has been shown to induce ecotoxicity to aquatic organisms at various trophic levels [8,9]. Pharmacological studies have shown that 46–62% of ATL is absorbed by the human body after oral administration and the unabsorbed fraction is excreted via urine, with 90% of ATL in the excreted substances present in their original form when detected in natural water [10]. Table 1 presents the basic physicochemical characteristics and chemical structure of ATL. Due to its high stability, the ATL removal efficiency is relatively low after treatment using physical, chemical, and biological processes in sewage treatment plants. Castiglioni et al. studied the removal treatment effectiveness for various pharmaceuticals in a sewage treatment plant in Italy [11], reporting an ATL removal efficiency in summer and winter of 55% and 10%, respectively, which was relatively low compared to other environmental contaminants. ATL is frequently detected in water due to its extensive usage and the difficulties presented in effective removal, with commonly detected concentrations in the $\text{ng}\cdot\text{g}^{-1}$ to $\mu\text{g}\cdot\text{g}^{-1}$ range [8]. Therefore, it is important to develop an environmentally friendly and effective technology for ATL degradation or removal from aquatic systems.

Table 1. Molecular structure of ATL.

Chemical Formula	Molecular Weight ($\text{g}\cdot\text{mol}^{-1}$)	Solubility (20 °C) ($\text{mg}\cdot\text{mL}^{-1}$)	Molecular Structure
$\text{C}_{14}\text{H}_{22}\text{N}_2\text{O}_3$	266.34	0.3	

Heterogeneous photocatalytic oxidation technology appears to be a promising treatment method for PPCPs, as semiconductors can be irradiated to produce electron-hole pairs and generate powerful and non-selective hydroxyl radicals during the process. Hydroxyl radicals can degrade most macromolecular organic pollutants with complex structures into non-toxic organic or inorganic matter with a lower molecular weight. Nano- TiO_2 semiconductors have become increasingly popular as photocatalysts, since their capacity for photocatalytic water splitting was [12]. TiO_2 semiconductors possess the properties of non-toxicity, biochemical stability, large surface area, and cost-effectiveness. When the nano- TiO_2 photocatalyst is irradiated by photons with energy greater than or equal to the bandgap energy of 3.2 eV, an electron (e_{cb}^-) from the valence band will migrate to the conduction band, leaving holes (h_{vb}^+) in the valence band [13]. The h_{vb}^+ can then directly oxidize ATL adsorbed on the surface of TiO_2 , as well as react with H_2O and OH^- to generate hydroxyl radicals (OH), resulting in improved ATL De due to their strong oxidizing capability [14]. Numerous previous studies have shown that UV/ TiO_2 photocatalysis is an effective technique for the removal of antibiotics from aquatic environments. However, one of the major limitations to the practical application of this technique is the requirement for a UV light source, commonly in the form of low- and medium-pressure mercury lamps, which are fragile, bulky, radiate high levels of heat, require long warm up times and waste high amounts of energy, while having a short working lifespan of 500–2000 h [15]. Additionally, the mercury UV lamp emits only fixed wavelengths within a very limited range and presents a risk of leakage of toxic materials [16]. Recently, the emergence of ultraviolet light emitting diode (UV-LED) technology has received much research attention and been applied to a wide range of applications due to its unique advantages of being environmentally friendly, exhibiting a long lifespan, and requiring short warm-up times and lower energy inputs due to the potential for operation at a moderate voltage.

LED lamp beads are very small, making them easy to install and transport. Furthermore, based on the material composition, the UV-LED emission wavelength can be varied and modern UV-LEDs are more powerful narrow-band devices which have a shorter relaxation time [17]. Therefore, compared to conventional UV light, UV-LED technology is more adjustable and applicable to wastewater treatment applications. For example, Cai et al. adopted UVA/LED/TiO₂ photocatalysis for the treatment of wastewater containing antibiotics and found that continuous UVA/LED/TiO₂ photocatalysis technology could remove >90% of 100 ppb sulfamethoxazole/trimethoprim [18]. Liang et al. found that the periodic illumination-controlled UV-LED/TiO₂ process was effective for PPCP degradation and removal, with reduced energy requirements when using porous titanium–titanium dioxide substrates [19]. Dal et al. found that UV-LED/TiO₂ processes were feasible for the decomposition of MB under suitable experimental conditions, demonstrating that UV-LEDs are effective as a light source for TiO₂ irradiation and has high potential for photodegradation [20]. Therefore, the UV-LED/TiO₂ process is a promising technique that has high potential in wastewater treatment [15,21,22].

To date, much research has been conducted on UV-LED/TiO₂ technology application in organic compound degradation, although ATL has rarely been studied as the target compound for the UV-LED/TiO₂ process. Ji et al. reported photocatalytic degradation of atenolol in aqueous TiO₂ suspensions [23]. However, this study was only under a mercury UV lamp, which may be different from UV-LED. Furthermore, it is essential to understand the influence of various environmental parameters on the degradation process mechanisms. Therefore, the photocatalytic performance of semiconductor-TiO₂ was investigated for ATL degradation using UV-LED irradiation. Batch experiments were performed to compare the effects of several environmental factors on ATL degradation efficiency, including catalyst crystal form (anatase TiO₂, rutile TiO₂, and mixed phase), catalyst dosage, UV-LED wavelength and intensity, pH, and co-existing anions and cations. The two main aims of this study were to: (1) investigate the feasibility of photocatalytic degradation of ATL using TiO₂ irradiated by UV-LED light; and (2) to determine the optimal operating conditions for practical application of UV-LED/TiO₂ technology.

2. Results and Discussion

2.1. Characterization of Anatase, Rutile, and Mixed Phase

We performed a SEM test to visualize the particle size of anatase, rutile and mixed phase. As shown in Figure 1a–c, the three kinds of TiO₂ have particle morphologies with particle sizes of 20–50, 50–100 and 20–50 nm, respectively. The X-ray powder diffraction pattern (XRD, Figure 1d) exhibits a typical anatase (JCPDS 89-4921), rutile (JCPDS 21-1276) and mixed crystalline phase, and no additional diffraction peaks of other species are observed. The content of rutile in mixed phase can be calculated by formula $X = 1/(1 + 0.8I_A/I_R)$, where X is the mass fraction of rutile phase, I_A is the intensity of the XRD peak of anatase phase $2\theta = 25.3$ degrees, and I_B is the intensity of the XRD peak of rutile phase $2\theta = 27.4$ degrees. Therefore, the ratio of anatase to rutile in mixed phase is estimated to be 83:17, which is close to Degussa P25 (80:20). The measurement of band gap is based on the method of reference [24]. The calculated E_g of these samples are 3.07, 3.01, and 3.03 eV (Tauc plots of the transformed Kubelka-Munk function vs. the energy, Inset of Figure 1e) of anatase, rutile and mixed phase, respectively. The N₂ adsorption-desorption test was supplemented to accurately determine the specific surface area of three kinds of TiO₂. As shown in Figure 1f, the BET surface areas were calculated to be 78.7, 32.2, and 102.6 m²/g of anatase, rutile, and mixed phase, respectively.

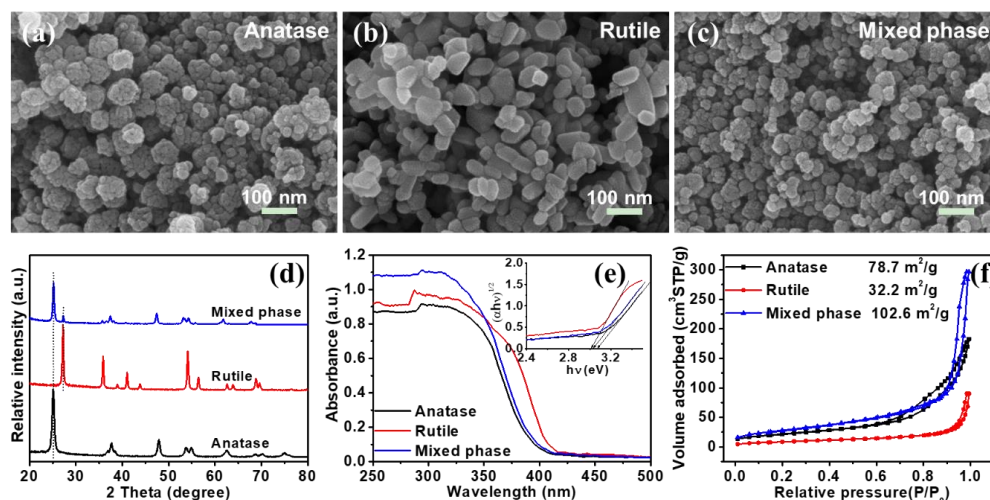


Figure 1. The SEM images (a–c), XRD patterns (d), UV–VIS DRS (e), Tauc plots (Inset) and N₂ adsorption-desorption isotherms (f) of anatase, rutile, and mixed phase.

2.2. Effect of the Nano-TiO₂ Crystal Form on ATL Degradation

The photocatalytic performance of the three different crystal forms of TiO₂ for ATL degradation, are shown in Figure 2. The De of mixed phase reached 100% within 60 min; while the ATL De was only 85.65% and 71.06% for anatase and rutile TiO₂, respectively. As shown in Figure 2b, the rate constant of mixed phase TiO₂ was almost 2–3-fold higher than that of anatase and rutile. In order to study the difference of charge separation of three kinds of TiO₂, we supplemented the measurement of surface photovoltage spectroscopy (Figure 2c, SPS). SPS is a powerful tool to further characterize charge separation at the nanoscale [25]. The surface photovoltage (SPV) response in mixed phase is obviously higher than that of anatase and rutile, revealing a dramatic increase in charge separation efficiency. Therefore, the mixed phase exhibits the highest activity, possibly due to its large specific surface area and excellent charge separation efficiency, and the influence of light absorption may not be significant. It has previously been proven that electronic interaction easily occurs between anatase and rutile TiO₂, with the electronic interaction between phases generating a mixed crystal lattice, causing the photocatalytic activity of the mixed crystalline nano-TiO₂ to be generally higher than that of the single-phase nano-TiO₂ [26].

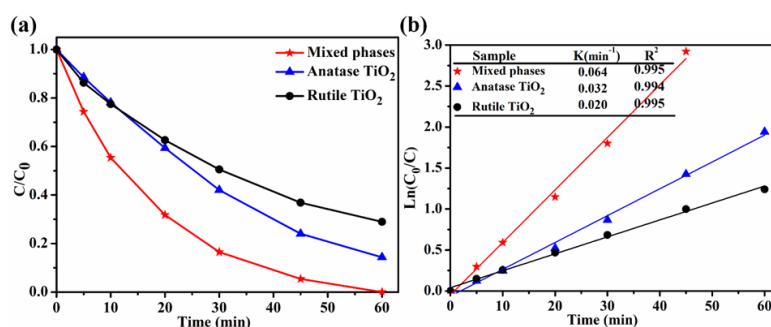


Figure 2. Cont.

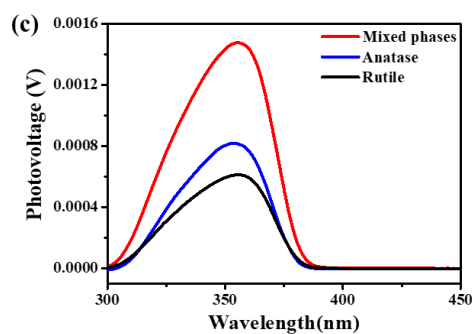


Figure 2. (a) De of ATL under different samples, (b) Pseudo- first-order model of ATL degradation. (c) the SPS test of anatase, rutile and mixed phase. Effect of nano-TiO₂ photocatalyst crystal phase on ATL degradation, with an initial ATL concentration of 18.77 μM and TiO₂ (anatase, rutile and mixed phase) concentration of 2.0 g/L; pH 7.6; Temperature 20 °C.

2.3. ATL Degradation by Combined UV-LED/Mixed Phase Process and Single UV-LED or Mixed Phase

The photocatalytic degradation of ATL was compared under different experimental conditions, including UV-LED, mixed phase, combined UV-LED and mixed phase, and a control blank (Figure 3). Results demonstrated that ATL concentrations showed a negligible decreased in the absence of UV-LED and TiO₂ photocatalyst or in the blank. ATL concentration decreased by 5% under conditions of TiO₂ alone, which may be attributed to fluctuation in the adsorption-desorption equilibrium due to the large surface area (102.6 m²/g) of the TiO₂ nano-powder. ATL was completely degraded by the synergistic effect of UV-LED and nano-TiO₂ photocatalysts after light irradiation for 60 min. These results indicate that photo-induced charge carriers were generated on the TiO₂ photocatalyst under UV-LED irradiation conditions. The photo-induced h⁺ then oxidized H₂O molecules to generate the active hydroxyl radical species, and the active radicals h⁺ and OH can oxidize ATL into carbon dioxide, water molecules, and other non-toxic small molecules. The specific mechanism is outlined in Equations (1)–(3). Furthermore, the pseudo-first-order kinetics model ($\ln \frac{C_0}{C} = kt$), was used to fit the obtained experimental data, showing a good fit for the photocatalytic degradation of ATL, while the R² value (>0.99) in the Figure 3b indicated good linearity of the fitted plots. UV-LED combined with TiO₂ displayed the highest k value of 0.0641 min⁻¹, while the rate constant for the control group remained low.

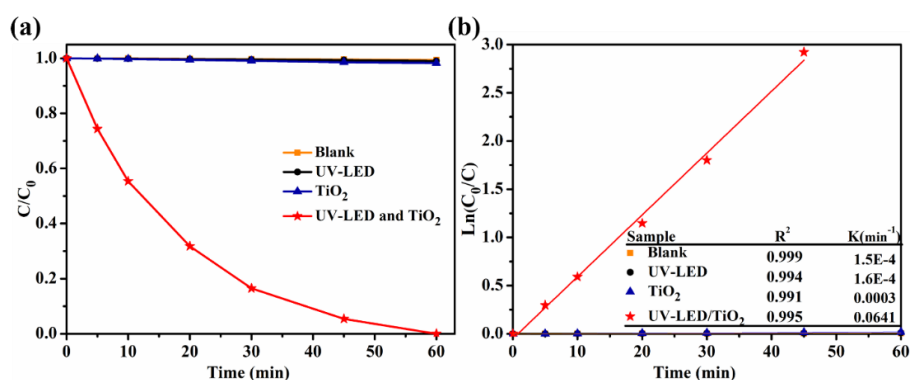
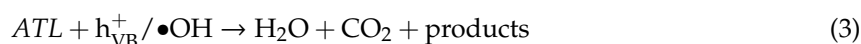


Figure 3. (a) ATL degradation efficiency under different conditions, (b) Pseudo- first-order model of ATL degradation. the initial ATL concentration of 18.77 μM and mixed phase concentration of 2.0 g/L; UV-LED wavelength: 365 nm; I₀ = 774 μW/cm²; pH: 7.6; temperature: 20 °C.

These results imply that UV-LED treatment combined with mixed phase TiO₂ photocatalysis is a feasible technique for ATL removal from the aqueous environment.

2.4. Effect of UV-LED Wavelength and Intensity on ATL Degradation

The influence of two different UV-LED emission wavelengths on ATL degradation is presented in Figure 4, the ATL De using a UV-LED light source with a wavelength of 365 nm was significantly higher than with a wavelength of 275 nm. The rate constant for 365 nm of 0.065 min⁻¹ being nearly nine-fold that of 275 nm. It can be seen from Figure 1e that the absorption of mixed phase at 275 and 365 nm is not very different, and the difference of their activity may not be the effect of absorption. On the contrary, the effect of light-induced charge separation may be significant. The electrochemical impedance spectroscopy (EIS) Nyquist plots of mixed phase under UV-LED at a wavelength of 365 and 275 nm are presented in Figure 4c. The charge transfer resistance at the catalyst/electrolyte interface could be evaluated by the semicircle radius of the Nyquist plots [27]. The smaller radius indicates that the charge transfer of the mixed phase at 365 nm is better than that at 275 nm, which may lead to higher activity at 365 nm. Overall, these results demonstrate that the mixed phase irradiated by UV-LED at a wavelength of 365 nm is a cost-effective and efficient method for ATL oxidization compared to irradiation at 275 nm.

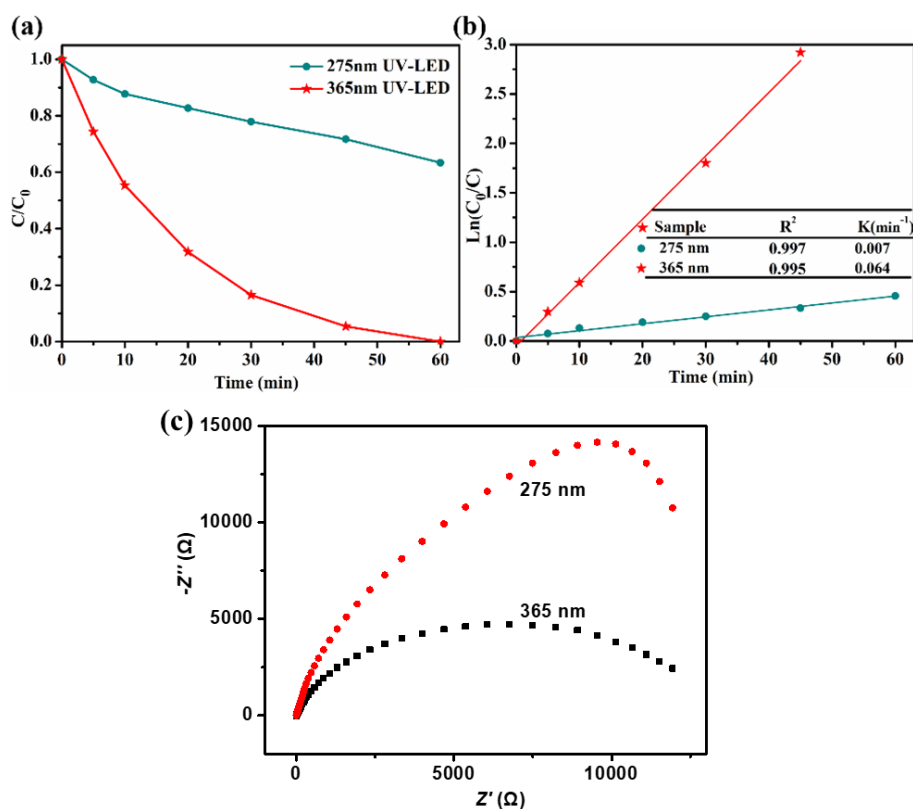


Figure 4. (a) Effect of varying UV-LED wavelengths on ATL degradation: $C(ATL)_0 = 18.77 \mu\text{M}$; (b) Pseudo-first-order model of ATL degradation. (c) the EIS of mixed phase under UV-LED at a wavelength of 365 and 275 nm. C mixed phase) = 2.0 g/L; $I_0 = 774 \mu\text{W}/\text{cm}^2$; pH: 7.6; temperature: 20 °C.

The UV-LED radiation intensity is an important parameter in the photocatalysis process, which directly determines the photon quantity in the photocatalytic system. The effect of varying light intensities (220, 332, 437, 551, 663, and 774 $\mu\text{W}/\text{cm}^2$) on the De of ATL were investigated and as shown in Figure 5, the ATL De increased with an increase in light intensity. ATL was completely degraded within 60 min under an irradiation intensity of 774 $\mu\text{W}/\text{cm}^2$, whereas only 57.23% of ATL was removed

under a light intensity of $220 \mu\text{W}/\text{cm}^2$. As shown in Figure 5b, the ATL degradation rate constant increased from 0.010 min^{-1} to 0.067 min^{-1} as the UV-LED light intensity increased from $220 \mu\text{W}/\text{cm}^2$ to $774 \mu\text{W}/\text{cm}^2$, showing an almost seven-fold increase. The increase in light intensity essentially relates to an increase in photon flux per reaction volume, resulting in an increase in the number of activated TiO_2 catalyst molecules per time unit. Consequently, electron transition in semiconductor TiO_2 occurred effectively under strong light intensities, causing more holes and hydroxyl radicals to be produced and, therefore, enhancing ATL degradation under these conditions. In addition, ATL degradation showed a relatively strong linear relationship with the UV-LED radiation intensity.

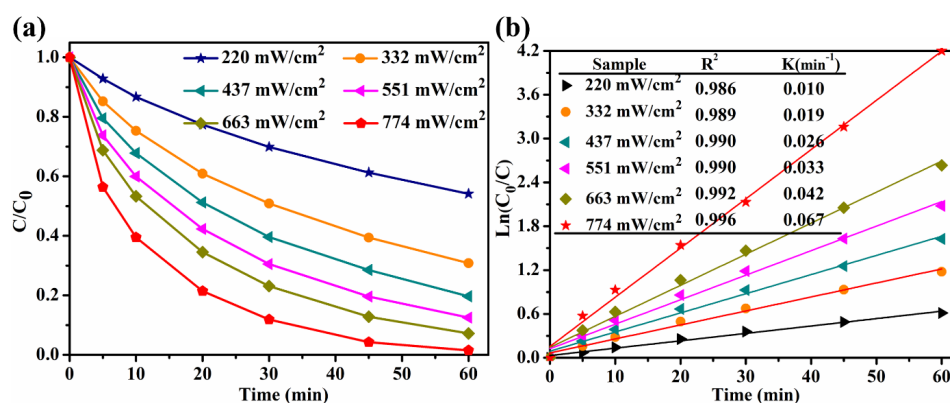


Figure 5. (a) Effect of varying UV-LED light intensities on ATL degradation, (b) Pseudo- first-order model of ATL degradation. initial ATL concentration of $18.77 \mu\text{M}$ and mixed phase concentration of 2.0 g/L ; pH: 7.6; temperature: $20 \text{ }^\circ\text{C}$.

2.5. Effect of the Initial ATL Concentration on Degradation Efficiency

The influence of the initial target compound concentration on the degradation process was assessed, with four different ATL concentrations ($9.39, 18.77, 28.16, 37.55 \mu\text{M}$). As shown in Figure 6, the ATL degradation rate constant decreased from 0.071 min^{-1} to 0.046 min^{-1} when the initial concentration of ATL increased from $9.39 \mu\text{M}$ to $37.55 \mu\text{M}$. This phenomenon occurs because the ATL molecules compete for the available hydroxyl radicals, with the insufficient availability of hydroxyl radicals causing the ATL degradation rate to decrease.

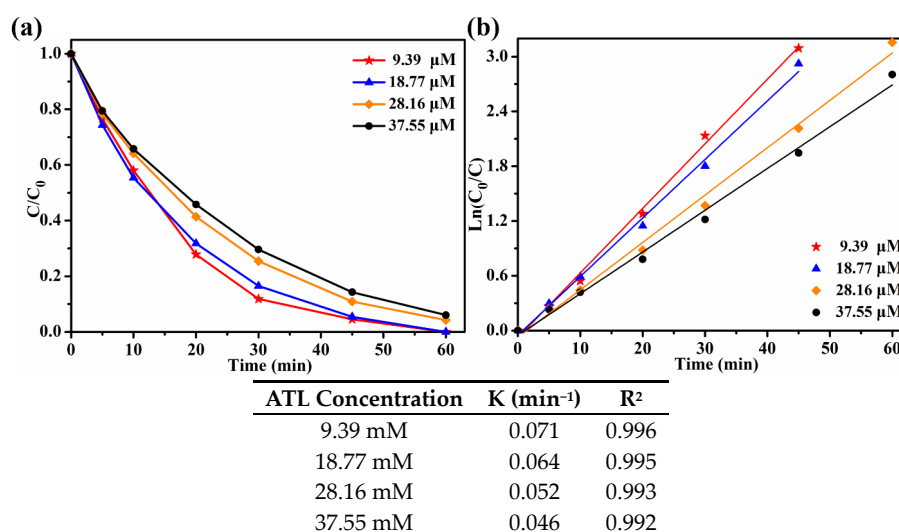


Figure 6. (a) Effect of varying initial concentration of ATL on ATL degradation (b) Pseudo- first-order model of ATL degradation. The initial mixed phase concentration of 2.0 g/L ; pH: 7.6; temperature: $20 \text{ }^\circ\text{C}$.

2.6. Effect of Mixed Phase Dosage on ATL Degradation

The influence of catalyst dosage on ATL degradation, was investigated by varying the initial photocatalyst mass concentration in the range of 0.2 g/L–2.8 g/L. The ATL degradation curve under different TiO₂ dosages is shown in Figure 7. The photocatalytic degradation of ATL was only 47.64% in 60 min when the catalyst dosage was 0.2 g/L, and the ATL De gradually reached a peak level when the TiO₂ dosage was increased to 2.0 g/L, achieving complete ATL degradation within 60 min. The ATL degradation efficiency then decreased with further increase in TiO₂ dosage from 2.0 g/L to 2.8 g/L. These results indicate that the ATL degradation rate did not increase linearly in accordance with TiO₂ concentration and that optimal ATL degradation at a rate constant of 0.064, was achieved at a TiO₂ concentration of 2.0 g/L. This was mainly because ATL degradation was dominated by the concentration of effective hydroxyl radicals (OH) in the photocatalytic system. When the mass concentration of nano-TiO₂ in solution was below the threshold of 2.0 g/L, more photoionization electron/hole pairs would be produced by increasing the TiO₂ dosage and therefore, the concentration of effective hydroxyl radicals would increase. However, when the TiO₂ dosage exceeds the threshold value of 2.0 g/L, UV light is scattered by an excess of TiO₂ particles in solution, reducing the penetration of UV light through water. Consequently, the light utilization efficiency is greatly reduced, leading to a low ATL De.

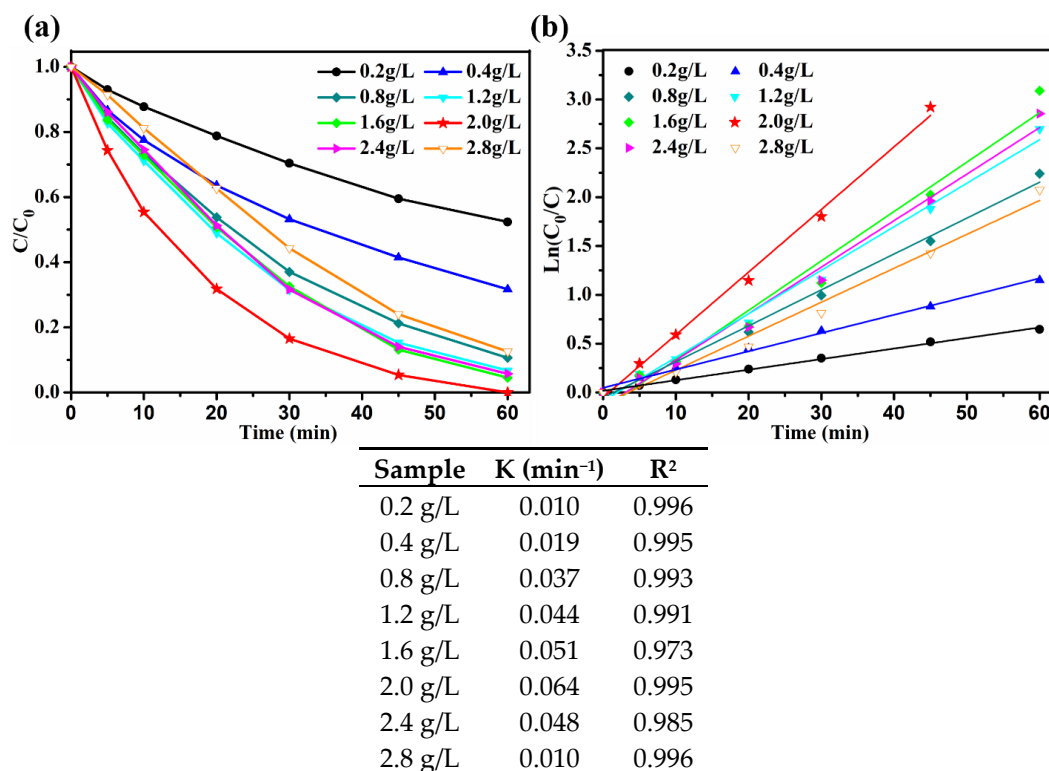


Figure 7. (a) Effect of varying nano-TiO₂ concentration on ATL degradation, (b) Pseudo-first-order model. The initial ATL concentration of 18.77 μM and mixed phase concentration of 2.0 g/L; pH: 7.6; temperature: 20 °C.

2.7. Effect of pH on ATL Degradation

In the photocatalytic oxidation process, the pH of the reaction system was found to have a significant influence on degradation of the target compound, mainly by affecting the formation of hydroxyl radicals in the system. The pH of the reaction solution was controlled to 3.0, 5.0, 7.0, 9.0, and 11.0 using phosphate buffer. ATL De under different pH conditions is shown in Figure 8. It can be observed that ATL De increased gradually as pH increased from 3.0 to 11.0. The ATL De was 92.11% at pH 3.0 after 60 min of UV-LED irradiation. When the pH was increased to 11.0, ATL was completely degraded

within only 30 min. The ATL degradation rate constant at pH 11 was 0.138 min^{-1} , which was 3.3-fold higher than at pH 3.0.

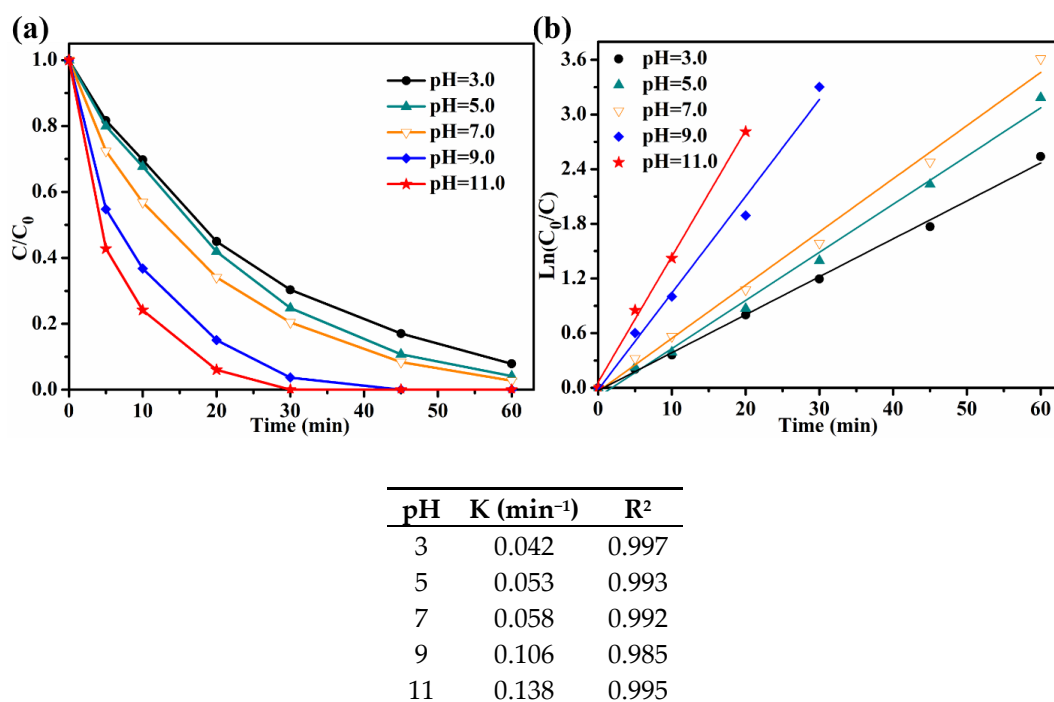
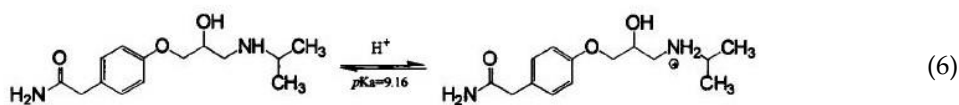


Figure 8. (a) Effect of pH on ATL degradation, (b) Pseudo-first-order model. The initial ATL concentration of $18.77 \mu\text{M}$ and mixed phase concentration of 2.0 g/L ; temperature: $20 \text{ }^\circ\text{C}$.

The influence of pH on the ATL degradation can be caused by the change in the charge state of the photocatalyst and the target compound [9]. The reaction equations for protonation and deprotonation of TiO_2 particles and ATL molecules in acidic or basic solutions are shown in Equations (4)–(6) [28]. Under acidic and neutral conditions, the surface of TiO_2 particles are positively charged after protonation and electrostatic repulsion occurs between TiO_2 particles and ATL molecules, which are also positively charged after protonation. This causes effective contact between ATL molecules and the TiO_2 photocatalyst to be greatly hindered, which inhibits the photocatalytic degradation of ATL. In contrast, the surface of TiO_2 particles were negatively charged after deprotonation in basic solutions, causing electrostatic attraction to ATL, which is in a neutral molecular state. Therefore, contact between ATL molecules and the photocatalyst is strengthened and photocatalytic degradation of ATL is promoted. Meanwhile, hydroxyl radicals ($\cdot\text{OH}$) were primarily generated by OH^- under basic conditions, as described in Equation (7) and the $\cdot\text{OH}$ generation efficiency was much higher than the process of $\cdot\text{OH}$ generation from H_2O . Therefore, the De of ATL can be substantially improved by increasing the pH of the aqueous environment.



2.8. Influence of Co-Existing Ions in the Aquatic Environment on ATL Degradation

Inorganic ions exist naturally in wastewater and environmental concentrations are usually reported in the range of 0.4–4 mM. Inorganic ions have different impacts on the photocatalytic degradation of target compounds. Some ions possess the ability to quench hydroxyl radicals and then generate new anion radicals by reacting with $\cdot\text{OH}$. Since the new free radicals will not be as powerful as OH , the photocatalytic reaction will be inhibited. However, some ions may generate $\cdot\text{OH}$ under UV light irradiation conditions, which can accelerate the photocatalytic reaction [29]. Therefore, it is necessary to investigate the specific influence of co-existing ions in aquatic environments, on the photocatalytic degradation of ATL by UV-LED irradiation.

As shown in Figure 9, the addition of Cl^- had almost had no influence on the ATL photodegradation process, while the addition of NO_3^- had a slight inhibitory effect on the photocatalytic process. SO_4^{2-} promoted ATL degradation to some degree, while the addition of CO_3^{2-} and HCO_3^- significantly promoted the photocatalytic degradation of ATL. Generally, CO_3^{2-} and HCO_3^- could react with hydroxyl radicals to generate less active carbonate radicals ($\text{CO}_3^{\cdot-}$) (Avisar et al., 2013) [30], affecting the amount of OH in the solution (Equations (8)–(9)). Therefore, it would be commonly presumed that the photocatalytic degradation of ATL would be inhibited in the presence of CO_3^{2-} and HCO_3^- , which is in contrast with these experimental results. In the present study, it was found that the hydroxyl radicals that reacted with CO_3^{2-} and HCO_3^- were primarily in the adsorbed state, which effectively reduced OH self-complexing prior to reacting with ATL, while hydroxyl radicals in their free state were less affected. Furthermore, due to the stability of $\text{CO}_3^{\cdot-}$ in solution its concentration could be enriched surrounding TiO_2 nanoparticles. The high concentration of $\text{CO}_3^{\cdot-}$ could compensate for the low activity of nano- TiO_2 particles, accelerating the diffusion of TiO_2 nanoparticles into the reaction system, increasing contact with ATL molecules, consequently promoting ATL degradation. Hu et al. reported promotion of the sulfamethoxazole photocatalytic degradation process by CO_3^{2-} and HCO_3^- , which was similar to the results of the present study [31]:

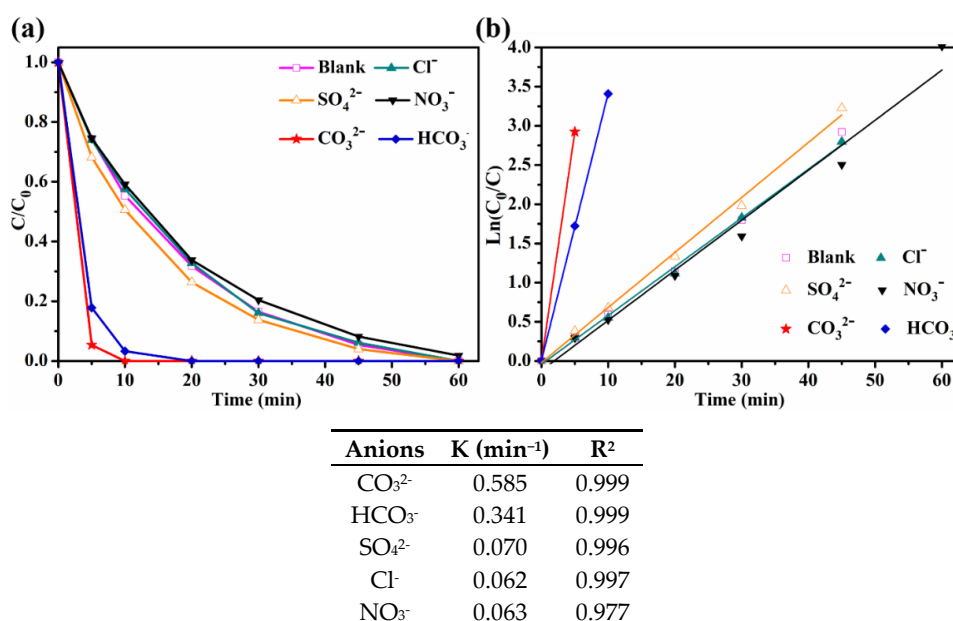
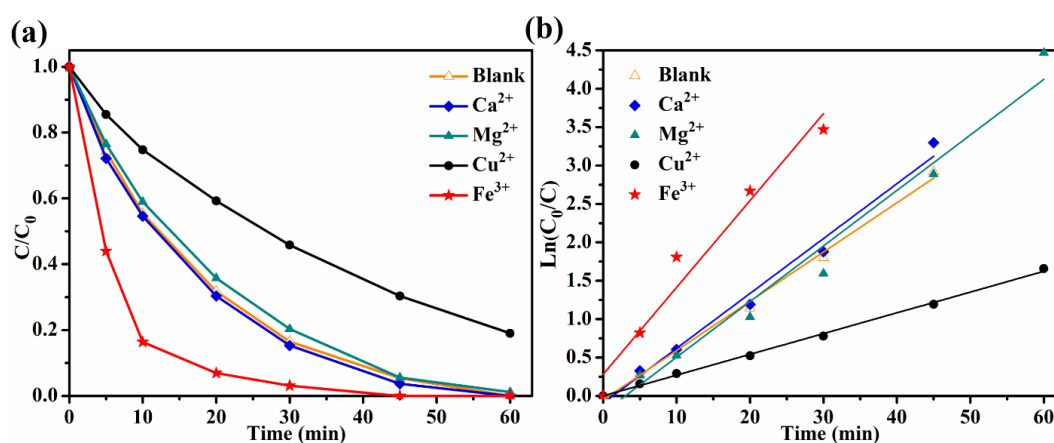


Figure 9. (a) Effect of co-existing anions in water on ATL degradation. (b) Pseudo- first-order model.

The effect of four commonly co-existing cations on ATL degradation are shown in Figure 10. The addition of Ca^{2+} ions induced no significant effect on ATL degradation, while the presence of Mg^{2+} caused a slight inhibition to ATL degradation. Among all the metal ions, the addition of Cu^{2+} had the most obvious inhibitory effect on ATL degradation. Fe^{3+} ions had the most significant effect, causing a promotion of ATL degradation, with 100% ATL degradation observed within 45 min. The pseudo-first-order kinetic model showed that when the concentration of Cu^{2+} in solution was 1 mM, the ATL degradation rate constant was 0.027 min^{-1} , while the rate constant increased to 0.1132 min^{-1} when the concentration of Fe^{3+} was 1 mM. Compared with the blank control, the ATL degradation rate was reduced by 57.9% with the addition of Cu^{2+} ions, while increasing by 1.76-fold due to the addition of Fe^{3+} ions. The inhibition of Cu^{2+} ions could be caused by the following reasons: (1) Cu^{2+} ions can easily become recombination centers for valence band holes and conduction band electrons in the photocatalytic system, which improves the recombination efficiency of photoinduced electron-hole pairs and affects the amount of holes and derived hydroxyl radical in the system. (2) Cu^{2+} ions in the solution could capture electrons and be transformed into elemental Cu, which is extremely unstable. Elemental Cu can easily be oxidized into Cu^{2+} by reacting with holes and hydroxyl radicals in the system (Equations (10)–(11)), thereby reducing the amount of active species in the system. (3) Cu^{2+} ions have the capacity to absorb UV light, leading to a decreased number of photons arriving and absorbing on the surface of the TiO_2 photocatalyst, potentially reducing ATL degradation. The promoting effect of Fe^{3+} ions on ATL photocatalytic degradation may be attributed to Fe^{3+} capture of photo-generated electrons on the surface of nano- TiO_2 catalysts, which effectively improves the separation efficiency of holes and electrons. Furthermore, the addition of Fe^{3+} ions could initiate a Fenton-like reaction, increasing the amount of free hydroxyl radicals in the reaction system and resulting in a significant improvement in ATL degradation:



Cations	K (min^{-1})	R ²
Fe^{3+}	0.113	0.949
Ca^{2+}	0.071	0.984
Mg^{2+}	0.072	0.971
Blank	0.064	0.995
Cu^{2+}	0.027	0.997

Figure 10. (a) Effect of co-existing cations in water on ATL degradation. (b) Pseudo- first-order model.

2.9. Influence of Free Radical Scavenging on ATL Degradation

In the UV-LED photocatalytic degradation reaction system, OH radicals are the dominant active species because of its non-selective strong oxidizing properties [32,33]. The influence of OH on photocatalytic ATL degradation was investigated by the addition of different concentrations of tert-butanol (TBA) to the reaction solution, as a free radical scavenger. The ATL De in the presence of different concentrations of TBA, is shown in Figure 11. Results show that TBA has a relatively low affinity to nano-TiO₂ particles and can react rapidly with OH. Meanwhile, TBA can suppress the free radical reaction chain and intensively compete for OH involved in ATL degradation. As shown in Figure 10, the addition of TBA significantly inhibited the photocatalytic degradation of ATL and the inhibition effect was enhanced with increasing TBA concentrations. When the TBA concentration was 10 mM, the ATL degradation efficiency was only 19.91% after UV-LED irradiation for 60 min. However, when the TBA concentration was increased to 50 mM, the ATL degradation efficiency under the same conditions was only 4.58%, indicating that the ATL degradation process was significantly inhibited under these conditions. When the concentration of TBA was 10 mmol/L, the pseudo-first-order kinetic model results suggested that the degradation of ATL was 0.0037 min⁻¹, which is only 5.76% of the ATL degradation observed in the control experiment. With an increase in TBA concentration the ATL degradation rate continued to decrease, suggested that TBA is an effective OH quencher and that OH radicals were a major contributor to the photocatalytic degradation of ATL under UV-LED irradiation conditions. Although the holes in the valence band of TiO₂ have oxidative ability, they were not found to contribute significantly to ATL degradation due to the weak adsorption capacity of ATL onto the nano-TiO₂ surface. In addition, the oxidative ability of holes was not found to be as powerful as that of OH. Nevertheless, hydroxyl radicals (OH) generated via the oxidation of H₂O and OH⁻ ions by valence band holes could diffuse throughout the whole reaction system and play a key role in the photocatalytic degradation of ATL.

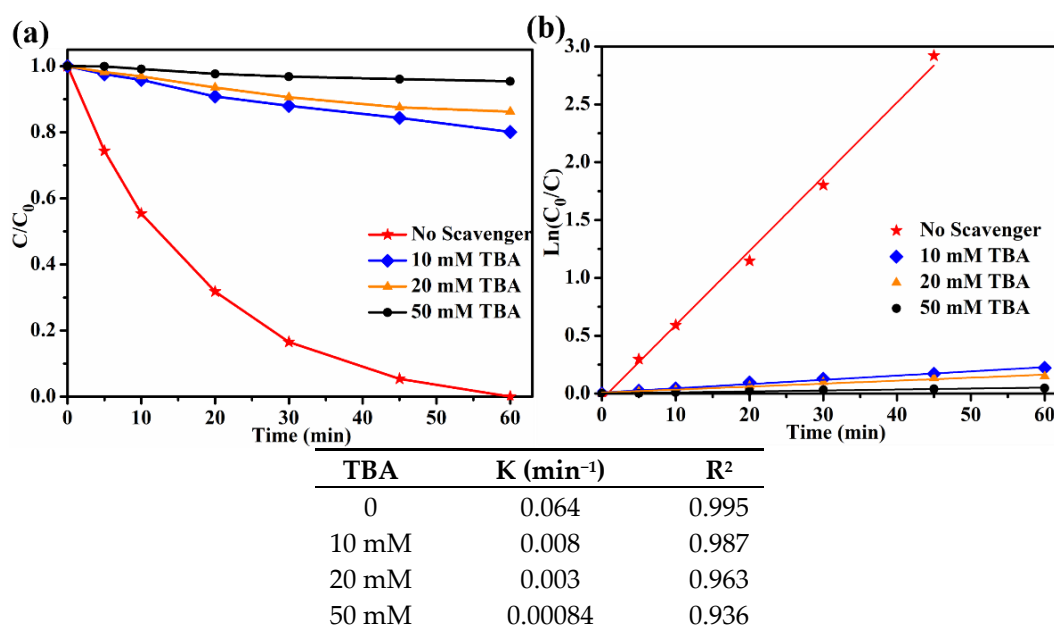


Figure 11. (a) Effect of free radical inhibition by varying concentrations of TBA on ATL degradation. (b) Pseudo-first-order model.

2.10. Comparison with Other Reports

Although photocatalytic degradation of pollutants by TiO₂ has been extensively studied, there are few reports of utilizing UV-LED to degrade atenolol (Table 2). In our study, atenolol was degraded by mixed phase TiO₂, and the degradation efficiency could reach 100% within the next hour under

UV-LED. Compared with high-pressure mercury lamp, the use of UV-LED is more environmentally friendly, but also greatly reduces the cost of operation. Moreover, the production cost of commercial TiO₂ is simple, the total cost is greatly reduced, and the possibility of later practical application is greatly improved, which has practical application significance. More importantly, most of the degradation of atenolol is using mercury lamps and xenon lamps, while our research offers possibilities for its application under UV-LED.

Table 2. The comparison of mixed phase TiO₂ with other reported TiO₂ photocatalysts towards photocatalytic decomposition of atenolol.

Catalyst	Light Source	Atenolol Concentration	Degradation Time	Ref.
Degussa P25	Xe lamp	15 mg/L	4 h	[34]
Degussa P25	High-pressure mercury lamp	37.6 μM	1 h	[23]
Ag-TiO ₂	High-pressure mercury lamp	20 mg/L	0.5 h	[35]
TiO ₂ /Salicylaldehyde-NH ₂ -MIL-101(Cr)	Xe lamp	10 mg/L	5 h	[36]
Immobilized TiO ₂	High-pressure mercury lamp	10 mg/L	5 h	[37]
Aeroxide TiO ₂ P25	Low-pressure mercury lamp	50 μM	1 h	[38]
Mixed phase TiO ₂	UV-LED	18.77 μM	1 h	This work

3. Materials and Methods

3.1. Materials

ATL (purity ≥98%) was from Shandong Xiya Chemical Industry Co. (Jinan, China), with a 187.73 μmol/L stock solution prepared and serially diluted as required for experiments. Methanol (HPLC grade) was from Merck KG (Germany). The pH was adjusted using 0.1 M HClO₄, NaOH and phosphate buffer. All other reagents used in experiments were of analytical grade and were from Sionpharm Chemical Reagent Shanghai Co. (Shanghai, China). All experimental solutions were prepared using ultrapure water with a resistivity of 18.2 MΩ·cm produced using a Millipore Milli-Q ultrapure water system.

Three commercially-available nano-TiO₂ types with different crystal forms were compared as catalysts. Pure anatase TiO₂, pure rutile TiO₂, and mixed crystal type TiO₂ were purchased from Shandong Xiya Chemical Co. (Jinan, China). and the characteristics of the nano-TiO₂ materials are given in Table 3.

Table 3. Characteristics of nano-TiO₂ semiconductor.

Crystal Form	Composition	Particle Size (nm)	BET Surface Area (m ² /g)
Anatase	100% anatase	20–50	78.7
Rutile	100% rutile	50–100	32.2
Mixed phase	83% anatase + 17% rutile	20–50	102.6

3.2. Experimental Setup

The photocatalytic degradation reaction was carried out in an open plexiglass container with a volume of 500 mL. After stirring for 60 min in the dark to reach the adsorption equilibrium, the solution was illuminated under UV-LED irradiation (Table 4). The outer wall of the reactor was tightly wrapped with a layer of aluminum foil, to prevent scattering of light energy, heat energy or

radiation. The reactor had a circular irradiation window with a diameter of ~5 cm at the light source. The irradiation light source consisted of two sets of custom built UV-LED units, with operational wavelengths of 275 nm and 365 nm. The UV-LED light irradiated vertically into the reactor through the light source irradiation window, ensuring that all lamp beads were below the upper limit level of the reaction mixture. The temperature during the photocatalytic reaction was maintained at 20 ± 0.5 °C using a cryostat, with cooling water continuously circulated around the outer wall of the reactor. The luminous flux entering the reactor was measured using a UV light meter. A schematic of the photocatalytic reaction device is illustrated in Figure 12.

Table 4. Different experimental variables regarding atenolol photodegradation with TiO₂ photocatalyst under UV-LED.

	Photocatalysts	Illumination	pH	ATL Concentration	Co-Existing Ions	TBA
2.2	2.0 g/L of mixed phase, anatase, rutile	365 nm; 774 uW/cm ²	7.6	18.77 uM	None	None
2.3	2.0 g/L of mixed phase	365 nm; 774 uW/cm ²	7.6	18.77 uM	None	None
2.4	2.0 g/L of mixed phase	275/365 nm; 774 uW/cm ²	7.6	18.77 uM	None	None
2.5	2.0 g/L of mixed phase	365 nm; 220–774 uW/cm ²	7.6	9.39–37.55 uM	None	None
2.6	2.8 g/L of mixed phase	365 nm; 774 uW/cm ²	7.6	18.77 uM	None	None
2.7	2.0 g/L of mixed phase	365 nm; 774 uW/cm ²	3–11	18.77 uM	None	None
2.8	2.0 g/L of mixed phase	365 nm; 774 uW/cm ²	7.6	18.77 uM	1 mM of CO ₃ ²⁻ , HCO ₃ ⁻ , SO ₄ ²⁻ , NO ₃ ⁻ , Cl ⁻ , Ca ²⁺ , and Mg ²⁺ , Fe ³⁺ , Cu ²⁺	None
2.9	2.0 g/L of mixed phase	365 nm; 774 uW/cm ²	7.6	18.77 uM	None	0–50 mM

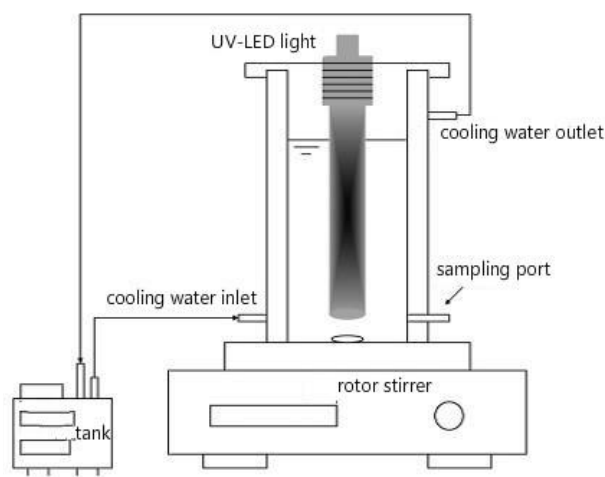


Figure 12. Schematic of the photocatalytic reaction device.

3.3. Analytical Method

During the photocatalytic process, samples of the suspension were withdrawn at certain time intervals and filtered through a 0.22 µm syringe filter. The ATL concentration was measured using a high-performance liquid chromatograph (HPLC, Waters e2695) [39] equipped with a Symmetry C18 column (4.6 mm × 250 mm, 5.0 µm) manufactured by Waters Scientific (USA). The mobile phase consisted of 87% methanol and 13% 0.01 MKH₂PO₄ at pH 2.5, with an injection volume of 20 µL. The column temperature was maintained at 35 °C, with a flow rate of 1 mL/min. The detection wavelength for ATL was 229 nm.

4. Conclusions

In this study, ATL photocatalytic degradation was investigated using nano-TiO₂ as photocatalyst under UV-LED irradiation. The influence of several environmental factors on ATL degradation efficiency were systematically investigated via batch experiments, including the catalyst crystal form (anatase TiO₂, rutile TiO₂ and mixed phase), catalyst dosage, UV-LED wavelength and intensity, co-existing anions and cations, pH, and radical scavenger concentration. The specific mechanism of effect was investigated for all factors and the following conclusions were drawn based on the experimental results:

- (1) The mixed phase exhibits the highest activity, possibly due to its large specific surface area and excellent charge separation efficiency, and the influence of light absorption may not be significant.
- (2) ATL can be effectively degraded using mixed phase TiO₂ combined with UV-LED technology and the ATL degradation efficiency could reach 100% for 60 min. The photocatalytic reaction process could be explained via pseudo-first order kinetics;
- (3) ATL photodegradation was more effective under 365 nm UV-LED than 254 nm, which was caused by the effect of light-induced charge separation.
- (4) The enhancement of UV-LED irradiation intensity could significantly facilitate ATL degradation by increasing the number of effective photons to the TiO₂ surface. The ATL degradation rate constant at 774 μW/cm² was 0.067 min⁻¹, which was 6.7-fold higher than that at 220 μW/cm² (0.010 min⁻¹).
- (5) The highest ATL degradation efficiency was achieved at an optimal TiO₂ catalyst dosage of 2.0 g/L in the photocatalytic system, inducing complete degradation of ATL in 60 min.
- (6) The pH significantly affects the protonation and charge of semiconductor TiO₂, leading to a fluctuation of hydroxyl radical concentrations in the reaction system. The ATL degradation efficiency increased with increasing pH, with complete degradation within 30 min at pH 11.0. The ATL degradation rate constant increased from 0.0409 min⁻¹ to 0.1423 min⁻¹ when the pH was increased from 3.0 to 11.0.
- (7) The ATL degradation efficiency decreased with an increase in initial ATL concentration.
- (8) The presence of co-existing ions significantly affected ATL degradation by altering the amount of hydroxyl radicals. Co-existing anions, such as SO₄²⁻, NO₃⁻, Cl⁻, Ca²⁺, and Mg²⁺, exerted a negligible influence on ATL degradation, while the addition of CO₃²⁻, HCO₃⁻, and Fe³⁺ ions significantly promoted photocatalytic ATL degradation, and Cu²⁺ ions strongly inhibited the ATL degradation process.
- (9) OH were found to be the dominant active species in UV-LED photocatalytic degradation of ATL.

Author Contributions: Conceptualization: Z.R. and S.L.; methodology: L.W. and Y.F.; validation: S.L. and C.M.; formal analysis: L.W. and Y.F.; investigation: Z.R. and S.L.; writing—original draft preparation: Z.R., L.W., and Y.F.; writing—review and editing: Z.R., S.L., and C.M.; supervision: Z.R. and C.M.; project administration: Z.R. and C.M.; funding acquisition: Z.R. and S.L.

Funding: This research was jointly funded by the key consulting project of the Shenzhen Science and Technology Program (JCYJ20160226092135176, GJHZ20180416164721073), the project of the Shenzhen Institute of Information Technology (PT201703), the Innovation and Enhancing College Project of Guangdong Province, (2017GKTSCX065), the National Science Foundation of China (51508383), and the Natural Science Foundation of Tianjin Province (18JCQNJC09000).

Conflicts of Interest: The authors declare no conflict of interest.

References

1. Ellis, J. Pharmaceutical and personal care products (PPCPs) in urban receiving waters. *Environ. Pollut.* **2006**, *144*, 184–189. [[CrossRef](#)] [[PubMed](#)]
2. Jacobs, H.E.; Haarhoff, J. Prioritisation of parameters influencing residential water use and wastewater flow. *J. Water Supply Res. Technol.* **2007**, *56*, 495–514. [[CrossRef](#)]

3. Liu, J.-L.; Wong, M.-H. Pharmaceuticals and personal care products (PPCPs): A review on environmental contamination in China. *Environ. Int.* **2013**, *59*, 208–224. [[CrossRef](#)] [[PubMed](#)]
4. Hofmann, R.; Amiri, F.; Wilson, S.; Garvey, E.; Metcalfe, C.; Ishida, C.; Lin, K. Comparing methods to remove emerging contaminants and disinfection by-product precursors at pilot scale. *J. Water Supply Res. Technol.* **2011**, *60*, 425–433. [[CrossRef](#)]
5. Kwon, J.W.; Rodriguez, J.M. Occurrence and removal of selected pharmaceuticals and personal care products in three wastewater-treatment plants. *Arch. Environ. Contam. Toxicol.* **2014**, *66*, 538–548. [[CrossRef](#)]
6. Xie, R.; Meng, X.; Sun, P.; Niu, J.; Jiang, W.; Bottomley, L.; Li, D.; Chen, Y.; Crittenden, J. Electrochemical oxidation of ofloxacin using a TiO₂-based SnO₂-Sb/polytetrafluoroethylene resin-PbO₂ electrode: Reaction kinetics and mass transfer impact. *Appl. Catal. B Environ.* **2017**, *203*, 515–525. [[CrossRef](#)]
7. Constantinescu, G.; Theodoros, D.; Russell, T.; Ward, E.; Wilson, S.; Wootton, R. Treating disordered speech and voice in Parkinson's disease online: a randomized controlled non-inferiority trial. *Int. J. Lang. Commun. Disord.* **2011**, *46*, 1–16.
8. Alder, A.C.; Schaffner, C.; Majewsky, M.; Klasmeier, J.; Fenner, K. Fate of β -blocker human pharmaceuticals in surface water: Comparison of measured and simulated concentrations in the Glatt Valley Watershed, Switzerland. *Water Res.* **2010**, *44*, 936–948. [[CrossRef](#)]
9. Hapeshi, E.; Achilleos, A.; Vasquez, M.I.; Michael, C.; Xekoukoulotakis, N.; Mantzavinos, D.; Kassinos, D.; Xekoukoulotakis, N. Drugs degrading photocatalytically: Kinetics and mechanisms of ofloxacin and atenolol removal on titania suspensions. *Water Res.* **2010**, *44*, 1737–1746. [[CrossRef](#)]
10. Karaman, R.; Dajani, K.; Hallak, H. Computer-assisted design for atenolol prodrugs for the use in aqueous formulations. *J. Mol. Mod.* **2012**, *18*, 1523–1540. [[CrossRef](#)]
11. Castiglioni, S.; Bagnati, R.; Fanelli, R.; Pomati, F.; Calamari, D.; Zuccato, E. Removal of Pharmaceuticals in Sewage Treatment Plants in Italy. *Environ. Sci. Technol.* **2006**, *40*, 357–363. [[CrossRef](#)] [[PubMed](#)]
12. Fujishima, A.; Honda, K. Electrochemical Photolysis of Water at a Semiconductor Electrode. *Nature* **1972**, *238*, 37–38. [[CrossRef](#)] [[PubMed](#)]
13. Tachikawa, T.; Fujitsuka, M.; Majima, T. Mechanistic Insight into the TiO₂ Photocatalytic Reactions: Design of New Photocatalysts. *J. Phys. Chem. C* **2007**, *111*, 5259–5275. [[CrossRef](#)]
14. Joo, J.; Kwon, S.G.; Yu, T.; Cho, M.; Lee, J.; Yoon, J.; Hyeon, T.; Lee, J. Large-Scale Synthesis of TiO₂ Nanorods via Nonhydrolytic Sol–Gel Ester Elimination Reaction and Their Application to Photocatalytic Inactivation of *E. coli*. *J. Phys. Chem. B* **2005**, *109*, 15297–15302. [[CrossRef](#)]
15. Ye, Y.; Feng, Y.; Bruning, H.; Yntema, D.; Rijnaarts, H. Photocatalytic degradation of metoprolol by TiO₂ nanotube arrays and UV-LED: Effects of catalyst properties, operational parameters, commonly present water constituents, and photo-induced reactive species. *Appl. Catal. B Environ.* **2018**, *220*, 171–181. [[CrossRef](#)]
16. Kneissl, M.; Seong, T.-Y.; Han, J.; Amano, H. The emergence and prospects of deep-ultraviolet light-emitting diode technologies. *Nat. Photonics* **2019**, *13*, 233–244. [[CrossRef](#)]
17. Korovin, E.; Selishchev, D.; Besov, A.; Kozlov, D. UV-LED TiO₂ photocatalytic oxidation of acetone vapor: Effect of high frequency controlled periodic illumination. *Appl. Catal. B Environ.* **2015**, *163*, 143–149. [[CrossRef](#)]
18. Cai, Q.; Hu, J. Effect of UVA/LED/TiO₂ photocatalysis treated sulfamethoxazole and trimethoprim containing wastewater on antibiotic resistance development in sequencing batch reactors. *Water Res.* **2018**, *140*, 251–260. [[CrossRef](#)]
19. Liang, R.; Van Leuwen, J.C.; Bragg, L.M.; Arlos, M.J.; Fong, L.C.L.C.; Schneider, O.M.; Zurakowsky, I.J.; Fattahi, A.; Rathod, S.; Peng, P.; et al. Utilizing UV-LED pulse width modulation on TiO₂ advanced oxidation processes to enhance the decomposition efficiency of pharmaceutical micropollutants. *Chem. Eng. J.* **2019**, *361*, 439–449. [[CrossRef](#)]
20. Dai, K.; Lu, L.; Dawson, G. Development of UV-LED/TiO₂ Device and Their Application for Photocatalytic Degradation of Methylene Blue. *J. Mater. Eng. Perform.* **2013**, *22*, 1035–1040. [[CrossRef](#)]
21. Eskandarian, M.R.; Choi, H.; Fazli, M.; Rasoulifard, M.H. Effect of UV-LED wavelengths on direct photolytic and TiO₂ photocatalytic degradation of emerging contaminants in water. *Chem. Eng. J.* **2016**, *300*, 414–422. [[CrossRef](#)]
22. Chen, H.-W.; Ku, Y.; Irawan, A. Photodecomposition of o-cresol by UV-LED/TiO₂ process with controlled periodic illumination. *Chemosphere* **2007**, *69*, 184–190. [[CrossRef](#)] [[PubMed](#)]

23. Ji, Y.; Zhou, L.; Ferronato, C.; Yang, X.; Salvador, A.; Zeng, C.; Chovelon, J.-M. Photocatalytic degradation of atenolol in aqueous titanium dioxide suspensions: Kinetics, intermediates and degradation pathways. *J. Photochem. Photobiol. A Chem.* **2013**, *254*, 35–44. [[CrossRef](#)]
24. D'Amato, C.A.; Giovannetti, R.; Zannotti, M.; Rommozzi, E.; Minicucci, M.; Gunnella, R.; Di Cicco, A. Band Gap Implications on Nano-TiO₂ Surface Modification with Ascorbic Acid for Visible Light-Active Polypropylene Coated Photocatalyst. *Nanomaterials* **2018**, *8*, 599. [[CrossRef](#)] [[PubMed](#)]
25. Kronik, L. Surface photovoltage phenomena: theory, experiment, and applications. *Surf. Sci. Rep.* **1999**, *37*, 1–206. [[CrossRef](#)]
26. Deiana, C.; Fois, E.; Coluccia, S.; Martra, G. Surface Structure of TiO₂P25 Nanoparticles: Infrared Study of Hydroxy Groups on Coordinative Defect Sites. *J. Phys. Chem. C* **2010**, *114*, 21531–21538. [[CrossRef](#)]
27. Macdonald, D.D. Reflections on the history of electrochemical impedance spectroscopy. *Electrochim. Acta* **2006**, *51*, 1376–1388. [[CrossRef](#)]
28. Pereira, J.H.; Reis, A.C.; Queirós, D.; Nunes, O.C.; Borges, M.T.; Vilar, V.J.; Boaventura, R.A. Insights into solar TiO₂-assisted photocatalytic oxidation of two antibiotics employed in aquatic animal production, oxolinic acid and oxytetracycline. *Sci. Total Environ.* **2013**, *463*, 274–283. [[CrossRef](#)]
29. Wang, L.; Guo, J.; Dang, J.; Huang, X.; Chen, S.; Guan, W. Comparison of the photocatalytic performance of TiO₂/AC and TiO₂/CNT nanocomposites for methyl orange photodegradation. *Water Sci. Technol.* **2018**, *78*, 1082–1093. [[CrossRef](#)]
30. Avisar, D.; Horovitz, I.; Lozzi, L.; Ruggieri, F.; Baker, M.; Abel, M.-L.; Mamane, H. Impact of water quality on removal of carbamazepine in natural waters by N-doped TiO₂ photo-catalytic thin film surfaces. *J. Hazard. Mater.* **2013**, *244*, 463–471. [[CrossRef](#)]
31. Hu, L.; Flanders, P.M.; Miller, P.L.; Strathmann, T.J. Oxidation of sulfamethoxazole and related antimicrobial agents by TiO₂ photocatalysis. *Water Res.* **2007**, *41*, 2612–2626. [[CrossRef](#)] [[PubMed](#)]
32. Pelaez, M.; Nolan, N.T.; Pillai, S.C.; Seery, M.K.; Falaras, P.; Kontos, A.G.; Dunlop, P.S.; Hamilton, J.W.; Byrne, J.; O'Shea, K.; et al. A review on the visible light active titanium dioxide photocatalysts for environmental applications. *Appl. Catal. B Environ.* **2012**, *125*, 331–349. [[CrossRef](#)]
33. Liu, Y.; Tian, L.; Tan, X.; Li, X.; Chen, X. Synthesis, properties, and applications of black titanium dioxide nanomaterials. *Sci. Bull.* **2017**, *62*, 431–441. [[CrossRef](#)]
34. Medana, C.; Calza, P.; Carbone, F.; Pelizzetti, E.; Hidaka, H.; Baiocchi, C. Characterization of atenolol transformation products on light-activated TiO₂ surface by high-performance liquid chromatography/high-resolution mass spectrometry. *Rapid Commun. Mass Spectrom.* **2009**, *23*, 206. [[CrossRef](#)]
35. Ling, Y.; Liao, G.; Xie, Y.; Yin, J.; Huang, J.; Feng, W.; Li, L. Coupling photocatalysis with ozonation for enhanced degradation of Atenolol by Ag-TiO₂ micro-tube. *J. Photochem. Photobiol. A Chem.* **2016**, *329*, 280–286. [[CrossRef](#)]
36. Mehrabadi, Z.; Faghihian, H. Comparative photocatalytic performance of TiO₂ supported on clinoptilolite and TiO₂/Salicylaldehyde-NH₂-MIL-101(Cr) for degradation of pharmaceutical pollutant atenolol under UV and visible irradiations. *J. Photochem. Photobiol. A Chem.* **2018**, *356*, 102–111. [[CrossRef](#)]
37. Arlos, M.J.; Hatat-Fraile, M.M.; Liang, R.; Bragg, L.M.; Zhou, N.Y.; Andrews, S.A.; Servos, M.R.; Maricor, J.A.; Melisa, M.H.-F.; Leslie, M.B.; et al. Photocatalytic decomposition of organic micropollutants using immobilized TiO₂ having different isoelectric points. *Water Res.* **2016**, *101*, 351–361. [[CrossRef](#)]
38. Ponkshe, A.; Thakur, P. Significant mineralization of beta blockers Propranolol and Atenolol by TiO₂ induced photocatalysis. *Mater. Today Proc.* **2019**, *18*, 1162–1175. [[CrossRef](#)]
39. Ravisankar, P.; Devala Rao, G.; Krishna Chaitanya, M.; Devadasu, C.H.; Srinivasa Babu, P. Rapid separation of five anti-hypertensive agents-atenolol, metoprolol, hydrochlorothiazide, amlodipine and nebivolol: Application to estimation of metoprolol succinate in tablet dosage form. *J. Chem. Pharm. Res.* **2013**, *5*, 215–228.

